Published in final edited form as:
Cell Calcium. 2009 March ; 45(3): 264–274. doi:10.1016/j.ceca.2008.11.005.

Alternative splicing of RyR1 alters the efficacy of skeletal EC coupling

Takashi Kimura[@,*], **John D. Lueck**[†,*], **Peta J. Harvey**[%], **Suzy M. Pace**[%], **Noriaki Ikemoto**[#], **Marco G. Casarotto**[%], **Robert T. Dirksen**[†,^], and **Angela F. Dulhunty**[%,^]

[%]John Curtin School of Medical Research, Australian National University, PO Box 334 Canberra, ACT, 2601, Australia

[@]Hyogo College of Medicine, 1-1 Mukogawa-cho Nishinomiya, HYOGO 663-8501, Japan

[†]University of Rochester, PO Box 711, 601 Elmwood Avenue, Rochester, NY, 14642

[#]Boston Biomedical Research Institute, Watertown, Massachusetts

Summary

Alternative splicing of ASI residues (Ala^{3481}-Gln^{3485}) in the skeletal muscle ryanodine receptor (RyR1) is developmentally regulated: the residues are present in adult ASI(+)RyR1, but absent in the juvenile ASI(-)RyR1 which is over-expressed in adult myotonic dystrophy type 1 (DM1). Although this splicing switch may influence RyR1 function in developing muscle and DM1, little is known about the properties of the splice variants. We examined excitation-contraction (EC) coupling and the structure and interactions of the ASI domain (Thr^{3471}-Gly^{3500}) in the splice variants. Depolarisation-dependent Ca^{2+} release was enhanced by >50% in myotubes expressing ASI(-)RyR1 compared with ASI(+)RyR1, although DHPR L-type currents and SR Ca^{2+} content were unaltered, while ASI(-)RyR1 channel function was actually depressed. The effect on EC coupling did not depend on changes in ASI domain secondary structure. Probing RyR1 function with peptides possessing the ASI domain sequence indicated that the domain contributes to an inhibitory module in RyR1. The action of the peptide depended on a sequence of basic residues and their alignment in an α-helix adjacent to the ASI splice site. This is the first evidence that the ASI residues contribute to an inhibitory module in RyR1 that influences EC coupling. Implications for development and DM1 are discussed.

1. Introduction

The ryanodine receptor (RyR) Ca^{2+} release channel contains two developmentally regulated splice regions, ASI and ASII [1]. The ASI residues (Ala^{3481}-Gln^{3485}) are lacking in the juvenile RyR1 isoform (ASI(-)RyR1), but present in the adult isoform (ASI(+)RyR1). Little is known about the properties of these splice variants, although it is attractive to consider that the isoforms are tailored to differential excitation-contraction (EC) coupling requirements in embryonic and adult muscle since the physical interaction between the dihydropyridine receptor (DHPR) and RyR1 that supports skeletal type EC coupling is established late in development [2]. The type 3 RyR (RyR3) is strongly expressed in neonatal skeletal muscle and supports EC coupling through Ca^{2+}-activated Ca^{2+} release [3,4]. The juvenile RyR1 splice variant is also expressed

Address for Correspondence Professor AF Dulhunty Division of Molecular Bioscience, John Curtin School of Medical Research, Australian National University, PO Box 334, Canberra City, ACT 2601, AUSTRALIA Phone +61 2 6125 4491 Fax +61 2 6125 4761 Email angela.dulhunty@anu.edu.au.
[*]made an equal first author contribution
[^]made an equal senior author contribution

but its contribution to neonatal EC coupling has not been assessed since the characteristics of EC coupling in the presence of ASI(-)RyR1 are not known. Therefore, we examined EC coupling in mytotubes expressing either ASI(-)RyR1 or ASI(+)RyR1.

Understanding the effects of the variable splicing is also important for understanding the myopathy in myotonic dystrophy type 1 (DM1), since the juvenile ASI(-)RyR1 splice variant is preferentially expressed in adults suffering from this disorder [5]. DM1 is caused by a CTG expansion in the 3' non-coding region of the myotonic dystrophy protein kinase (DMPK) gene, which leads to excess skeletal muscle excitability (myotonia) and muscle degeneration (myopathy). The myotonia is attributed to alternative splicing of ClC-1 mRNA [6-8] leading to loss of chloride channel function [9,10]. The myopathy is less well understood and attributed to a variety of causes including changes in EC coupling [11,12]. The impact of the juvenile RyR1 splice variant on EC coupling in DM1 has not been evaluated, once again because EC coupling has not been studied in muscle specifically expressing of this splice variant.

It seemed likely that the properties of EC coupling may be influenced by alternative splicing of the ASI region because the greater ASI region (Thr^{3471} - Gly^{3500}) is a significant regulatory domain. This is indicated by observations that changes in the ASI region: 1) influences RyR1 open probability [5], 2) contributes to an inhibitory module within RyR1 [14] and 3) binds to the DHPR β subunit [13]. The DHPR β subunit binds to a sequence of basic residues adjacent to the variably spliced residues and mutation of these basic residues results in depression of EC coupling [13]. This change in EC coupling has been attributed to disruption of DHPR β subunit binding to RyR1 [13], but could equally well be due to the mutation itself altering RyR1 activity during EC coupling. Indeed 4-chloro-*m*-cresol (4-CMC) responses shown in [13] suggest that mutation of basic β-binding residues drastically alters RyR1 responses to this ligand. Therefore, in addition to assessing the effect of the variable splicing on EC coupling and the secondary structure of the ASI domain, we have examined the role of the basic β-binding residues in determining structure of the ASI region and in regulating RyR1 activity. The role of these basic residues in regulating RyR1 activity was examined using the peptide probe approach used in previous studies that identified the ASI inhibitory module in RyR1 [14].

2. METHODS

2.1 Preparation and nuclear cDNA injections of dyspedic myotubes

Primary cultures and nuclear cDNA injections of myotubes from RyR1-null (dyspedic) mice were performed as previously described [5]. Co-injection of a cDNA encoding cherry red fluorescent protein (0.005μg/μl; [15]) was used to identify injected myotubes with excitation (540nm) using a monochrometer-based illumination system (TILL Photonics, Pleasanton, CA, USA).

2.2 Intracellular Ca^{2+} measurements in myotubes

Myotubes were loaded for 25min at room temperature with 5μM fura-FF AM (TEFLABS, Austin, TX, USA), a low to moderate affinity (K_d=5.5μM) Ca^{2+} dye, in a Ringer's solution containing: 146mM NaCl, 5mM KCl, 2mM $CaCl_2$, 1mM $MgCl_2$, 10mM HEPES, pH7.4. Fura-FF loaded myotubes were alternately excited at 340 and 380nm (510nm emission) every 350ms (8ms exposure per wavelength and 4×4 binning) using a monochrometer-based illumination system and captured using a high speed, digital QE CCD camera (TILL Photonics, Pleasanton, CA, USA). RyR1-mediated Ca^{2+} release was evoked using a 45s application of a maximal concentration (500μM) of 4-choro-m-cresol (4-cmc) and then reversed during a 60s wash with control Ringer's. Total store content was assessed during a 120s application of a 0 Ca^{2+} total store Ca^{2+} release cocktail (ICE) containing: 0.01mM ionomycin, 0.03mM cyclopiazonic acid

(CPA), and 2mM EGTA. Maximal fura-FF Ca^{2+} responses were evoked by subsequent application of a 10mM Ca^{2+} Ringer's solution in the continued presence of 0.01mM ionomycin to ensure that fura-FF was not saturated during prior 4-cmc or ICE applications.

2.3 Voltage clamp measurements

Voltage-gated L-type Ca^{2+} currents (L-currents) and intracellular Ca^{2+} transients were simultaneously recorded from ASI(+)RyR1- or ASI(-)RyR1-expressing myotubes using the whole-cell patch clamp technique as described previously [16]. For these experiments, the external solution contained: 145mM TEA-Cl, 10mM $CaCl_2$, and 10mM HEPES (pH7.4), and the pipette internal solution contained: 145mM Cs-aspartate, 0.1mM EGTA, 1.2mM $MgCl_2$, 0.2mM K_5-Fluo-4, 5mM Mg-ATP, and 10mM HEPES (pH7.4). Cell capacitance was determined by integration of the capacity transient resulting from a +10mV pulse applied from the holding potential and was used to normalize Ca^{2+} currents (pA/pF) from different myotubes. Fits to the voltage-dependence of L-current density and intracellular Ca^{2+} transients were performed using equations described previously [16]. The maximal rate of voltage-gated SR Ca^{2+} release was approximated from the peak of the first derivative of the fluo-4 fluorescence trace ($\delta F/\delta t$) elicited by a depolarisation to +60mV. The rate of change in fluo-4 fluorescence is an approximation of the maximal rate of Ca^{2+} release in myotubes because these cells exhibit a negligible Ca^{2+} removal flux [17].

2.4 Synthesis of domain peptides

Domain peptides were synthesized as described previously [14]. Stock solutions (5mM) were prepared in H_2O and frozen in 20µl aliquots.

RyR1 domain peptides

-ASI(+):	^{3471}TADSKSKMAKAGDAQSGGSDQERTKKKRRG^{3500}
-ASI(-):	^{3471}TADSKSKMAK----------SGGSDQERTKKKRRG^{3500}
- ASI(mutant):	^{3471}TADSKSKMAK----------SGGSDQERTAAKLRG^{3500}
-ASI(short):	^{3493}RTKKKRRG^{3500}
-DP4:	^{2422}LIQAGKGEALRIRAILRSLVPLDDLVGIISLPLQIP^{2477}

DHPR domain peptide

- Peptide ***A*** :	^{671}TSAQKAKAEERKRRKMSRGL^{690}

2.5 Nuclear Magnetic Resonance (NMR), circular dichroism (CD) and structural modelling

These structural techniques have been described previously [18]. Peptides (2mM) in 10% D_2O/90% H_2O adjusted to pH5.0 (HCl or NaOH) for NMR spectroscopy. Peptides were diluted to 50mM at pH5.0 for CD at 5°C on a Jobin Yvon CD6 Dichrograph (Cedex, France) using a cell path of 1mm. Ten spectra were collected per sample, averaged and subjected to a smoothing function. Structural models were constructed from NMR experiments, then energy minimized using the program Discover (Accelrys software Insight II), first by steepest descent and then by conjugate gradient until the maximum derivative was <0.001kcal/A.

2.6 [^{3}H]ryanodine binding and Ca^{2+} release

[^{3}H]ryanodine binding [14] to SR vesicles was assessed at 37°C in 100mM KCl, 20mM PIPES pH 6.8, 15nM [^{3}H]ryanodine, 1mM EGTA, 200µM AEBSF(4-(2-Aminoethyl)-

benzenesulfonyl fluoride hydrochloride) with appropriate [Ca^{2+}]. Ca^{2+} release was monitored at 710nm with the Ca^{2+} indicator, antipyrylazoIII. SR vesicles were added to 2ml of solution containing: 100mM KH_2PO_4 (pH7), 4mM $MgCl_2$; 1mM Na_2ATP; 0.5mM antipyrylazo III.

2.7 Single channel recording and analysis

Lipid bilayers were formed and vesicles incorporated using a *cis* (cytoplasmic) solution containing: 230mM $CsCH_3O_3S$, 20mM CsCl, 1.0mM $CaCl_2$, 10mM TES, and 500mM mannitol (pH7.4 with CsOH) and a *trans* (luminal) solution containing 30mM $CsCH_3O_3S$, 20mM CsCl, 1mM $CaCl_2$ and 10mM TES (pH7.4) [14]. Following RyR incorporation the *cis* solution was replaced with similar solution containing 100μM free [Ca^{2+}] and 200mM $CsCH_3O_3S$ was added to the *trans* solution to achieve a symmetrical 230mM $CsCH_3O_3S$ concentration. Current was recorded using an Axopatch 200 amplifier (Axon Instruments, Foster City, CA). Bilayer potential, V_{cis}-V_{trans} ($V_{cytoplasm}$-V_{lumen}), was switched between -40mV and +40mV every 30s. Channel activity was analysed over one to two 30s periods at -40mV and +40mV using the program Channel 2 (developed by PW.Gage and M.Smith, JCSMR). Threshold levels for channel opening were set to exclude baseline noise at ~20% of the maximum single channel conductance.

2.8 Statistics

Average data are given as mean ±S.E.M. An ANOVA analysis and post-hoc Dunnett's test was used to assess statistical significance ($P<0.05$) between groups in myotube experiments with $n\geq9$. For [^{3}H]ryanodine binding, Ca^{2+} release and single channel experiments, statistical significance was evaluated using paired or unpaired Student's t-test as appropriate when $n\geq3$. Numbers of observations (n) are given in Tables and Figure legends.

3. RESULTS

3.1 Influence of the ASI region on EC coupling

Ca^{2+} currents through the DHPR and Ca^{2+} release from the SR were recorded under voltage clamp conditions in dyspedic (RyR1-null) myotubes expressing either ASI(+)RyR1 or ASI(-)RyR1 (Fig. 1A). Voltage-activated Ca^{2+} release during EC coupling was significantly increased in myotubes expressing ASI(-)RyR1. However there was no difference in voltage sensor properties assessed from L-type Ca^{2+} currents. The substantial L-type Ca^{2+} currents in the ASI(+)RyR1 and ASI(-)RyR1 expressing myotubes (Fig. 1A) are in marked contrast to the minimal L-type currents observed in naïve dyspedic myotubes reported previously [19,20]. Fig. 1A shows representative L-type Ca^{2+} currents and intracellular Ca^{2+} transients elicited by 200ms depolarisations to the indicated potentials (-40mV to +60mV). The magnitude and voltage-dependence of L-type Ca^{2+} currents were similar in ASI(+)RyR1- and ASI(-)RyR1-expressing myotubes (Fig. 1B) and similar to those in normal myotubes [21]. Accordingly, maximal L-channel conductance (G_{max}) and the voltage for half-maximal L-channel activation ($V_{G1/2}$) were not different (Table 1, I-V data). Since the skeletal L-type Ca^{2+} current depends on a physical association between the DHPR and RyR1 [19], these results indicate that DHPR expression and RyR1 association is similar for ASI(+)RyR1 and ASI(-)RyR1.

In contrast to the similar RyR1-mediated enhancement in L-type Ca^{2+} current function in myotubes expressing ASI(+)RyR1 and ASI(-)RyR1, EC coupling was profoundly increased in ASI(-)RyR1-expressing myotubes when assessed either from the magnitude of depolarisation-induced Ca^{2+} transients (Fig. 1C) or the maximal rate of Ca^{2+} release (Fig. 1D&E). While the voltage for half-maximal activation ($V_{F1/2}$) was similar, maximal voltage-gated Ca^{2+} release ($(\Delta F/F)_{max}$) was significantly ($P<0.01$) increased in ASI(-)RyR1-expressing myotubes (Table 1, F-V data). A reasonable approximation of the maximum rate of SR Ca^{2+} release can be determined from the peak value of the first derivative of the Ca^{2+} transient

($\delta F/\delta t$) elicited by a strong depolarisation [20]. The maximal rate of SR Ca^{2+} release elicited at +60mV was significantly ($P<0.01$) higher in ASI(-)RyR1-expressing myotubes (Fig. 1D&E). It should be noted that the robust depolarisation-induced Ca^{2+} transients recorded from both ASI(+)RyR1 and ASI(-)RyR1-expressing myotubes are in marked contrast to the absence of such Ca^{2+} transients in naïve dyspedic myotubes [19]. In conclusion, the results show that voltage-gated Ca^{2+} release in increased in myotubes expressing ASI(-)RyR1, which lacks the variably spliced residues.

The enhanced voltage-gated Ca^{2+} release in ASI(-)RyR1 expressing myotubes is reminiscent of the greater activation of ASI(-)RyR1 by ASI peptides, which has been attributed to greater activation when the ASI inhibitory module is interrupted in ASI(-)RyR1 than in ASI(+)RyR1 [14]. The opening of RyR channels and skeletal muscle EC coupling is suggested by several studies to depend on changes in regulatory modules within the RyR [27-30]. Our results indicate that the ASI region is a part of a regulatory module that contributes to EC coupling and that release of this inhibition facilitates stronger EC coupling for ASI(-)RyR1 than ASI(+)RyR1.

3.2 The juvenile RyR1 splice variant does not alter SR Ca^{2+} store content, but does influence maximal 4-cmc-induced Ca^{2+} release

The greater voltage-gated Ca^{2+} release in ASI(-)RyR1-expressing myotubes could result from either a greater efficacy of DHPR-mediated Ca^{2+} release (EC coupling), a general increase in the RyR1 responsiveness to activating stimuli, and/or increased SR Ca^{2+} store content. Therefore, we determined the responsiveness of RyR1 to 4-cmc and the total releasable SR Ca^{2+} store content in non-injected dyspedic (RyR1-null) myotubes, ASI(+)RyR1- and ASI(-)RyR1-expressing myotubes. We have previously shown that caffeine-induced Ca^{2+} release is not significantly different in ASI(+)RyR1- and ASI(-)RyR1-expressing myotubes [5]. We used 4-cmc here both to explore the actions of a different agonist and because 4-cmc activates RyR1 and not RyR3 (which is expressed at low levels in myotubes) [22] so that the 4-cmc-induced Ca^{2+} responses can be definitively assigned to the expressed RyR1 variants. For these experiments, myoplasmic Ca^{2+} was measured using fura-FF, a low to moderate affinity (K_d=5.5μM) Ca^{2+} dye (which did not saturate during maximal release - see below). Addition of 4-cmc (500μM) elicited a rapid increase in intracellular Ca^{2+} in both ASI(+)RyR1- and ASI(-)RyR-expressing myotubes (Fig. 2A&B), but not in non-expressing dyspedic myotubes (Fig. 2B), demonstrating that release occurred through the expressed RyRs. In contrast to voltage-gated Ca^{2+} release (EC coupling), but consistent with single channel data [5], maximal 4-cmc-induced Ca^{2+} release was significantly reduced in ASI(-)RyR1-expressing myotubes (Fig. 2B, *left*).

To evaluate SR Ca^{2+} content, we used a Ca^{2+} release cocktail (ICE, containing zero Ca^{2+} - see Methods) to completely release Ca^{2+} from all intracellular stores, including SR, mitochondria, golgi and lysosomes. Given the relative size of each of these Ca^{2+} compartments (SR being ~75% of the total; [23]), this response is dominated by SR release. Addition of ICE revealed that the Ca^{2+} store content was not different between ASI(+)RyR1- and ASI(-)RyR1-expressing myotubes (Fig. 2B, *middle*). In contrast, and as expected, Ca^{2+} store content was significantly higher in non-expressing dyspedic myotubes, consistent with RyR1 channels contributing to a low level of uncompensated SR Ca^{2+} leak. A further increase in fura-FF ratio was observed following subsequent application of 10mM Ca^{2+} (Ca^{2+}, *dotted lines*, Fig. 2A), demonstrating that the dye was not saturated during the addition of either 4-cmc or ICE (Fig. 2B, *right*). To conclude, the absence of the variably spliced residues in ASI(-)RyR1 specifically inhibited Ca^{2+} release through the channel in response to 4-cmc. The changes in both resting RyR1 activity and in caffeine and 4-cmc induced activity with deletion of the ASI residues

([5] and Fig. 2) indicate that the inhibitory module containing the ASI residues influences resting channel activity as well as EC coupling.

The results in this and the previous section show that the two splice variants of RyR1 respond differently to the two types of triggers with ASI(-)RyR1 supporting a decreased release in response to exogenous triggers [caffeine and 4-cmc] and an increase in response to the endogenous DHPR-mediated trigger. This is a novel and physiologically important finding and provides strong evidence that the alternatively spliced region influences the strength of Ca^{2+} release during EC coupling, since release is increased in spite of a reduction observed for exogenous ligands.

3.3 The molecular structure of the ASI region

The observed effects on EC coupling may have been due to differential effects of the spliced residues on the secondary structure of the greater ASI domain. Therefore, we compared the structures of peptides comprising sequences flanking the ASI residues (Thr^{3471}-Gly^{3500}) in either the presence (peptide ASI(+)) or absence (peptide ASI(-)) of the variably spliced ASI residues (Methods). NMR proton assignments (Supplementary Table 1) were determined using TOCSY to identify spin types and NOESY for sequence assignments [24]. NOE cross-peaks indicate that two protons are separated by <5Å in an α-helical structure. Sequential (NH_i-NH_{i+1}, αH_i-NH_{i+1}, and βH_i-NH_{i+1}) and medium range (NH_i-NH_{i+2}, αH_i-βH_{i+3}, and αH_i-NH_{i+3}) NOE patterns (Fig. 3) indicated weak helix-like structures of 13-14 residues towards the C-terminus in both peptides. The degree of α-proton chemical shift deviation from tabulated random coil values [25] (not shown) and CD spectra were also consistent with the peptides having both helical and random coil structure. An ideal helix exhibits CD minima at 208 and 222nm [26]. The ASI(+) and ASI(-) peptides show a minimum at <208nm and weak inflections near 222nm (Fig. 4A). Fig. 4B shows structure predictions based on the NOE data with an α-helical region extending across 13-14 residues from the centre towards the C-terminus, including a contiguous sequence of basic residues, two of which are aligned along one surface of the helix. The N-terminal half of both ASI(+) and ASI(-) peptides (containing ASI residues in the ASI(+) peptide) is an extended coil. The similar structures of the ASI(+) and ASI(-) peptides suggest that functional differences between ASI(-)RyR1 and ASI(+)RyR1 cannot be attributed to different secondary structures in the ASI domain.

3.4 The sequence and structure of basic residues in the ASI peptides determines peptide function

The experiments in this section examine the structure and function of the ASI region in greater detail with a particular emphasis on the basic α-helical β-binding region downstream from the ASI residues. This region was of interest because mutation of these basic residues depresses EC coupling by ~60% [13] and because the basic sequence is similar that of peptide ***A,*** which also activates RyR1 [18,32-34].

A mutated ASI peptide (ASI(mutant)), with three of the basic residues replaced by either alanine or lysine - see methods) and a truncated peptide (ASI(short)) were synthesised. ASI (short) contained the basic residues but was likely to be too short to maintain a helical structure. Structural analysis showed that ASI(mutant) retained its helical structure, but without aligned basic residues which had been replaced with alanines. Structural analysis also confirmed that ASI(short), containing the basic residues, was unstructured (Fig. 3&4, Supplementary Table 1). The CD minimum at 195nm for ASI(short) in Fig. 4A also indicate that there is little helical structure.

The action of the peptides on native skeletal muscle RyR1 was compared using [^{3}H]ryanodine binding and Ca^{2+} release from SR vesicles. [^{3}H]ryanodine binding increases when channel

activity increases [31]. The ASI(-) peptide significantly increased both [^{3}H]ryanodine binding (Fig. 5A) and Ca^{2+} release (Fig. 5B&E). In contrast, the ASI(mutant) only marginally increased [^{3}H]ryanodine binding (Fig. 5A). The mutant peptide did not increase Ca^{2+} release at 10μM, but produced a small increase at 100μM (Fig. 5C&E). The small activation by ASI(mutant) was significantly less than the strong activation by the ASI(-) peptide at all peptide concentrations. These results indicate that all the basic residues are required for strong activation by the peptide. The helical structure is also important since [^{3}H]ryanodine binding was less with peptide ASI(short) than with ASI(-) at 100μM and 500μM (Fig. 5A) and Ca^{2+} release from SR was significantly reduced at all peptide concentrations (Fig. 5E). The mutation produced a generally stronger reduction in the effect of the peptide on both [^{3}H]ryanodine binding and Ca^{2+} release than the truncation, indicating that the negatively charged residues were the prime determinant of activation, but that their efficacy was greatly enhanced by their alignment in a helical structure.

ASI(short) in contrast to ASI(mutant) enhanced the later phase of Ca^{2+} release (1-3min after peptide addition, Fig. 5D). The late release is influenced both by the peptide and by the initial Ca^{2+} release, i.e. it contains a component of Ca^{2+}-induced Ca^{2+} release, whereas the initial release is solely peptide-dependent. Controls in this set of experiments were (a) the reduced activation of ASI(mutant) and ASI(short) provided controls for the specificity of the wild-type ASI peptide effects and (b) the increase in OD following addition of Ca^{2+} ionophore which was always observed (final arrows in Fig. 5B&D), indicated that Ca^{2+} remained in the SR vesicles and that antipyralazoIII was not saturated during peptide-evoked release.

In summary, the data in this section show that the basic α-helical β-binding residues are critically important in the activating action of the ASI peptides and that their helical structure is essential for maximal activation. The results further indicate that the basic residues adjacent to the ASI region are determinants of RyR1 activity, and therefore, may contribute to the enhancement of voltage dependent Ca^{2+} release during EC coupling, in addition to their role in binding the DHPR β-subunit [13]. Thus the two regions of the ASI domain influence RyR activity and EC coupling. Insertion of the variably spliced residues in ASI(+)RyR1 depresses voltage-dependent Ca^{2+} release (this study), while the presence of the basic residues facilitate EC coupling [13].

3.5 Effects of ASI peptides on RyR1 channels

The interaction between the wild-type and mutant peptides on single RyR channels was examined to further characterise the molecular nature of the peptide binding site. The ASI peptides strongly activate RyR1 at -40mV, but activate less at +40mV, where the bilayer voltage pushes the positively charged peptide into the pore. As a result, activation at low peptide concentrations is reduced at +40mV and channel activity can fall below control values, due to this non-specific inhibitory action observed at higher peptide concentrations [14]. These effects are clearly seen with ASI(-) in Fig. 6A&C, with significant activation by AS1(-) at -40mV and significant inhibition by 100μM peptide at +40mV. ASI(short) on the other hand failed to increase RyR1 activity at -40mV, but strongly blocked activity at +40mV when applied at 100μM, with a greater potency than ASI(-)(Fig. 6B&C). The ASI(mutant) peptide had no effect on channel activity (not shown), consistent with its minimal effects on [^{3}H]ryanodine binding and Ca^{2+} release from SR (Fig. 5). The channel data suggest that the reduced effect of ASI (short) on [^{3}H]ryanodine binding and Ca^{2+} release from the SR is a combination of lower activation plus maintained inhibition at higher peptide concentrations.

3.6 The ASI peptides and peptide A

There is a remarkable similarity between the structure and function of the ASI peptides and a peptide (peptide ***A***) corresponding to the A region of the DHPR II-III loop [18,32-34]. The

similar structures are shown in Fig. 4. The ASI peptides and peptide ***A*** each activate RyR1 at -40mV and high concentrations inhibit RyR1 at +40mV. Activation by ASI peptides and peptide ***A*** each depends on the alignment of positively charged residues in an α-helical structure. In addition, RyR1 activation by peptide ***A*** is affected by either truncation or mutation of positive residues [18] in a manner that is almost identical to the effects of truncation or mutation of ASI(-). Because of these similarities, we hypothesized that the ASI peptides and peptide ***A*** might interrupt the same inhibitory module in RyR1. The possibility was explored with competition studies (Fig. 7). The ASI(+) and ASI(-) peptides alone each significantly increased [^{3}H]ryanodine binding (Fig. 7A&B, solid lines), but failed to significantly increase [^{3}H]ryanodine binding if channels were first activated by 100μM peptide ***A*** (Fig. 7A&B, broken lines). The activation by 100μM peptide ***A*** alone is seen by the enhanced activity with zero ASI peptide - i.e. the first diamond data point in Figs 7A and B. This was not due to saturation of ryanodine binding to native RyR1 channels since binding of >250% control was achievable in this preparation with 10μM caffeine plus 100μM peptide ***A*** or ASI(-) in the presence of 10μM Ca^{2+} (Fig. 7C).

As a control for the specificity of the peptide ***A*** in blocking the ASI effects, an active but structurally unrelated domain peptide (DP4 peptide (Leu^{2442}-Pro^{2477})) [35,36] was added with 500μM ASI(-). Ryanodine binding with 500μM ASI(-) was 190±1% of control, binding with 100μM DP4 was 236±13% of control and binding with 500μM ASI(-) plus 100μM DP4 was 339±32% control. Thus, as expected and in contrast to peptide ***A***, the effects of DP4 and ASI (-) were additive and independent. A final control experiment for the specificity of the ASI and peptide ***A*** competition was performed with the unrelated activator, caffeine. The actions of both ASI(-) and peptide ***A*** were additive with the effects of caffeine indicating, again as expected, that the peptides and caffeine act independently (Fig. 7C).

The remarkable overlap between the effects of ASI peptides and peptide ***A*** was explored further by comparing the effects on Ca^{2+}-dependent activation of RyR1 by the two peptides with the effects of the unrelated DP4 domain peptide. ASI(+), ASI(-), and peptide ***A*** each significantly increased [^{3}H]ryanodine binding at [Ca^{2+}]s ≥10μM (Fig. 8A). As previously reported [14] the ASI(-) peptide produced significantly greater activation than ASI(+). Activation by peptide ***A*** was significant but not significantly different from activation by ASI(+). Neither peptide ***A*** nor the ASI peptides altered activation by Ca^{2+} as a percentage of maximum binding (Fig. 8B). In contrast to the ASI peptides and peptide ***A***, DP4 significantly reduced the [Ca^{2+}] required for RyR1 activation (Fig. 8A&B, also reported by [35]). Ryanodine binding with 1μM Ca^{2+} was significantly greater in the presence of DP4 than in the absence of peptide or in the presence of ASI peptides and peptide ***A***. The [Ca^{2+}] required for 50% activation fell from 3-4μM without peptide or with the ASI peptides and peptide ***A***, to ~400nM with DP4. On the other arm of the Ca^{2+} activation curve, DP4 rendered the RyR less sensitive to Ca^{2+} inhibition, with <20% inhibition by 1mM Ca^{2+} in the presence of this peptide, compared with ≥50% inhibition under all other conditions. In conclusion, the ASI peptides and peptide ***A*** had very similar effects on Ca^{2+}-dependent RyR1 activation that was very different from the effect imposed by DP4.

Overall, the results in this section suggest that the ASI peptides and peptide ***A*** share a common binding site on RyR1 by virtue of their similar amino acid sequences and α-helical structures that aligns basic residues along one surface of the α-helix.

4.0 DISCUSSION

This study describes several novel observations. Firstly, we have identified a variably spliced region in RyR1 that profoundly effects skeletal muscle EC coupling and is thus are likely to participate in the poorly understood but crucial mechanism that transmits the EC coupling

signal from the DHPR to the RyR1 channel pore. These particular residues have not previously been implicated in EC coupling. Secondly, this is the first report that variable splicing of RyR1 alters skeletal muscle EC coupling. Thirdly, the newly defined two dimensional structure of the ASI domain provides a structural basis for understanding the contribution of the ASI region to both EC coupling and a critical inhibitory module within RyR1. Fourthly, we show the basic residues in RyR1 involved in binding the β subunit of the DHPR [13] also influence intrinsic gating of the RyR1 ion channel. Finally, we show that ASI domain peptides and the ***A*** region of the DHPR II-III loop exhibit analogous secondary structures and activate RyR1 by competing for a common site. The results have significant implications not only for EC coupling but also for Ca^{2+} regulation in developing skeletal muscle and the myopathy in DM1.

4.1 The involvement of the ASI region in basal RyR1 channel activity and EC coupling

The lower basal [5] and 4-cmc-induced ASI(-)RyR1 activity (Fig. 2) can be explained by a stronger intramolecular inhibitory module in ASI(-)RyR1 than in ASI(+)RyR1. This assertion is supported by peptide probe studies where (a) the ASI peptides activate ASI(-)RyR1 more than ASI(+)RyR1 and (b) the ASI(-) peptide produced greater activation of native and recombinant RyR1 channels than the ASI(+) peptide [14]. The greater activation by the ASI (-) peptide could be explained if the ASI(-) sequence bound strongly and suggested that the same sequence in ASI(-)RyR1 may form a stronger inhibitory module than that in ASI(+)RyR1 [14]. The inhibitory module is presumably formed by an interaction between the ASI domain and other regions of RyR1. The results further show that the basic DHPR β subunit binding domain adjacent to the variably spliced residues is critical for the contribution of the ASI region to the inhibitory module. The degree of inhibition is modulated by the presence or absence of the variably spliced residues.

Since the resting ASI(-)RyR1 channel activity is ~20% less than that of ASI(+)RyR1 [14], we considered that resting cytoplasmic [Ca^{2+}] might be lower and the SR Ca^{2+} content higher in the ASI(-)RyR1-expressing myotubes. However this was not the case. Both resting cytoplasmic Ca^{2+} [5] and SR Ca^{2+} content (Fig. 2B) are similar in cells expressing either isoform. Therefore, other mechanisms including sarcolemmal, SR, and mitochondrial Ca^{2+} transport must compensate for the difference in basal RyR1 activity. This is analogous to malignant hyperthermia mutations in RyR1 that produce mild increases in RyR1 activity but are not sufficient to alter net SR Ca^{2+} content [16].

4.2 Structure and function of the ASI peptides

The secondary structure of the ASI(+) and ASI(-) peptides is very similar, with NMR and CD both indicating helix-like characteristics. The N-terminal half of each peptide is random coil and the C-terminus of both peptides contains a 13-15 residue amphipathic helix with two basic residues extending from one face. The ability of the ASI peptides to activate RyR1 channels in bilayers depends on the helical alignment of these basic residues. The similar α-helical structures and alignment of basic residues in ASI(-) and ASI(+) suggest that a tighter interaction in the ASI(-) inhibitory module may reflect size and charge differences rather than structural differences. In addition, it is possible that conformational forces on the ASI region in the RyR1 tetramer may induce structural changes that contribute to the differences observed between the two isoforms of the channel.

Our hypothesis is that the α-helical basic residues adjacent to the ASI variably spliced residues form the critical binding site for the AS1 region. These residues are present in both the ASI(+) and ASI(-) peptides. We propose that both peptides bind and activate RyR1, but do so with different affinities based on the presence or absence of the adjacent ASI residues. In other words, the absence of the variably spliced residues in ASI(-) facilitates the association between the basic residues and the binding site on RyR1.

4.3 The role of the basic α-helical region in EC coupling

The strength of skeletal EC coupling is markedly reduced by deletion of the cluster of positively charged amino acids (K^{3495}KKRR__R^{3502}) that are immediately adjacent to the alternatively spliced ASI residues [13]. Although this was attributed to a disruption to binding of the β_{1a}-subunit [13], it is possible that the deletion also interrupted the ASI inhibitory module. Our peptide probe studies with ASI(mutant) (Figs 5&6) suggest that deletion of K^{3495}KKRR__R^{3502} would disrupt the inhibitory module and this could depress EC coupling, by analogy to the hypothetical ability of the tighter inhibitory module in ASI(-)RyR1 [14] to facilitate EC coupling (Fig. 1). It is possible that mutation of the K^{3495}KKRR__R^{3502} residues removes two critical regulatory components of the EC coupling pathway. Indeed, both deletion of K^{3495}KKRR_R^{3502} [13] and inclusion of the alternatively spliced ASI residues (Fig. 1) each reduce Ca^{2+} release during EC coupling without shifting its voltage dependence, consistent with the two interventions acting via a common mechanism. We suggest that increased Ca^{2+} release during EC coupling observed in ASI(-)RyR1-expressing myotubes could result either from an effect of the ASI residues on the activity of the ASI domain inhibitory module during voltage sensor activation, the strength of β_{1a}-subunit binding to RyR1 and regulation of EC coupling, or to a combination of the two effects. Distinguishing between these possibilities will require further experimentation, however preliminary data suggest that the β_{1a}-subunit binding is similar for ASI(-)RyR1 and ASI(+)RyR1 (Karunasekara Y, Beard NA, Pouliquin P, Poux A, & Dulhunty AF, unpublished).

4.4 Implications of ASI(-)RyR1 activity in development and DMI

The strong response of ASI(-)RyR1 to depolarisation may help in establishing a Ca^{2+}-independent EC coupling during development. The Ca^{2+} release units that facilitate skeletal muscle (Ca^{2+}-independent) EC coupling are formed during E16-18 [2] at a time when RyR3 (which supports Ca^{2+}-induced Ca^{2+}-release) and ASI(-)RyR1 (which supports Ca^{2+}-independent EC coupling) are co-expressed [1,37] (see Introduction). We speculate that the impact of tightly voltage-regulated Ca^{2+} release through ASI(-)RyR1 would be enhanced by the strong response of this isoform to depolarisation. Later, when RyR3 expression is reduced and there is an abundance of RyR1, voltage-activated Ca^{2+} via ASI(+)RyR1 would dominate.

The myopathy in DM1 has been attributed to factors including altered: (a) protein synthesis [38] (b) contractile protein expression and force generating capacity [39,40], (c) Ca^{2+}-calmodulin-dependent protein kinase activity and phosphorylation of phospholamban [39] and (d) ATP turnover [41]. Additionally, while ASI(-)RyR1 expression is increased in DM1, the mechanism by which lowered resting RyR1 channel activity could contribute to the myopathy was unclear [5]. The altered efficiency of DHPR-RyR1 coupling described here could well contribute to the myopathy if increased Ca^{2+} release during EC coupling resulted in excess Ca^{2+} accumulation in micro-domains that promote muscle degeneration through activation of Ca^{2+}-dependent proteases (e.g. calpain).

Supplementary Material

Refer to Web version on PubMed Central for supplementary material.

5. ACKNOWLEDGEMENTS

We thank Dr. P.D. Allen for access to dyspedic mice. The work was supported by grants from the Australian National Health and Medical Research Council (#316937 to AFD) and the National Institute of Health (AR44657 to RTD).

8. REFERENCES

1. Futatsugi A, Kuwajima G, Mikoshiba K. Tissue-specific and developmentally regulated alternative splicing in mouse skeletal muscle ryanodine receptor mRNA. Biochem J 1995;305(Pt 2):373–8. [PubMed: 7832748]
2. Takekura H, Flucher BE, Franzini-Armstrong C. Sequential docking, molecular differentiation, and positioning of T-Tubule/SR junctions in developing mouse skeletal muscle. Dev Biol 2001;239:204–14. [PubMed: 11784029]
3. Sorrentino V, Reggiani C. Expression of the ryanodine receptor type 3 in skeletal muscle. A new partner in excitation-contraction coupling? Trends Cardiovasc Med 1999;9:54–61. [PubMed: 10189968]
4. Chun LG, Ward CW, Schneider MF. Ca^{2+} sparks are initiated by Ca^{2+} entry in embryonic mouse skeletal muscle and decrease in frequency postnatally. Am J Physiol Cell Physiol 2003;285:C686–97. [PubMed: 12724135]
5. Kimura T, Nakamori M, Lueck JD, et al. Altered mRNA splicing of the skeletal muscle ryanodine receptor and sarcoplasmic/endoplasmic reticulum Ca^{2+}-ATPase in myotonic dystrophy type 1. Hum Mol Genet 2005;14:2189–2200. [PubMed: 15972723]
6. Kimura T, Takahashi MP, Okuda Y, et al. The expression of ion channel mRNAs in skeletal muscles from patients with myotonic muscular dystrophy. Neurosci Lett 2000;295:93–6. [PubMed: 11090982]
7. Mankodi A, Takahashi MP, Jiang H, et al. Expanded CUG repeats trigger aberrant splicing of ClC-1 chloride channel pre-mRNA and hyperexcitability of skeletal muscle in myotonic dystrophy. Mol Cell 2002;10:35–44. [PubMed: 12150905]
8. Charlet BN, Savkur RS, Singh G, Philips AV, Grice EA, Cooper TA. Loss of the muscle-specific chloride channel in type 1 myotonic dystrophy due to misregulated alternative splicing. Mol Cell 2002;10:45–53. [PubMed: 12150906]
9. Lueck JD, Lungu C, Mankodi A, et al. Chloride channelopathy in myotonic dystrophy resulting from loss of posttranscriptional regulation for CLCN1. Am J Physiol Cell Physiol 2007;292:C1291–7. [PubMed: 17135300]
10. Lueck JD, Mankodi A, Swanson MS, Thornton CA, Dirksen RT. Muscle chloride channel dysfunction in two mouse models of myotonic dystrophy. J Gen Physiol 2007;129:79–94. [PubMed: 17158949]
11. Orizio C, Esposito F, Paganotti I, Marino L, Rossi B, Veicsteinas A. Electrically-elicited surface mechanomyogram in myotonic dystrophy. Ital J Neurol Sci 1997;18:185–90. [PubMed: 9323511]
12. Siciliano G, Rossi B, Rosellini P, Muratorio A. Changes in muscular excitability and contractility caused by fatigue in Steinert's disease. Riv Neurol 1990;60:250–3. [PubMed: 2100052]
13. Cheng W, Altafaj X, Ronjat M, Coronado R. Interaction between the dihydropyridine receptor Ca^{2+} channel beta-subunit and ryanodine receptor type 1 strengthens excitation-contraction coupling. Proc Natl Acad Sci U S A 2005;102:19225–30. [PubMed: 16357209]
14. Kimura T, Pace SM, Wei L, Beard NA, Dirksen RT, Dulhunty AF. A variably spliced region in the type 1 ryanodine receptor may participate in an inter-domain interaction. Biochem J 2007;401:317–24. [PubMed: 16989644]
15. Shaner NC, Campbell RE, Steinbach PA, Giepmans BN, Palmer AE, Tsien RY. Improved monomeric red, orange and yellow fluorescent proteins derived from Discosoma sp. red fluorescent protein. Nat Biotechnol 2004;22:1567–72. [PubMed: 15558047]
16. Dirksen RT, Avila G. Distinct effects on Ca^{2+} handling caused by malignant hyperthermia and central core disease mutations in RyR1. Biophys J 2004;87:3193–204. [PubMed: 15347586]
17. Garcia J, Beam KG. Measurement of calcium transients and slow calcium current in myotubes. J Gen Physiol 1994;103:107–23. [PubMed: 8169594]
18. Casarotto MG, Gibson F, Pace SM, Curtis SM, Mulcair M, Dulhunty AF. A structural requirement for activation of skeletal ryanodine receptors by peptides of the dihydropyridine receptor II-III loop. J Biol Chem 2000;275:11631–7. [PubMed: 10766780]
19. Nakai J, Dirksen RT, Nguyen HT, Pessah IN, Beam KG, Allen PD. Enhanced dihydropyridine receptor channel activity in the presence of ryanodine receptor. Nature 1996;380:72–5. [PubMed: 8598910]
20. Avila G, Dirksen RT. Rapamycin and FK506 reduce skeletal muscle voltage sensor expression and function. Cell Calcium 2005;38:35–44. [PubMed: 15955561]

21. Avila G, O'Connell KM, Groom LA, Dirksen RT. Ca^{2+} release through ryanodine receptors regulates skeletal muscle L-type Ca^{2+} channel expression. J Biol Chem 2001;276:17732–8. [PubMed: 11278546]
22. Fessenden JD, Wang Y, Moore RA, Chen SR, Allen PD, Pessah IN. Divergent functional properties of ryanodine receptor types 1 and 3 expressed in a myogenic cell line. Biophys J 2000;79:2509–25. [PubMed: 11053126]
23. Fryer MW, Stephenson DG. Total and sarcoplasmic reticulum calcium contents of skinned fibres from rat skeletal muscle. J Physiol 1996;493(Pt 2):357–70. [PubMed: 8782101]
24. Wuthrich, K. NMR of Proteins and Nucleic Acids. Wiley; New York: 1986.
25. Wishart DS, Sykes BD, Richards FM. Relationship between nuclear magnetic resonance chemical-shift and protein secondary structure. Journal of Molecular Biology 1991:311–333. [PubMed: 1960729]
26. Woody RW, Tinoco I. Optical rotation of oriented helices 3. Calculation of rotatory dispersion and circular dichrism of alpha- and 3-10 helix. Journal of Chemical Physics 1967;46
27. Ikemoto N, Yamamoto T. Postulated Role of Inter-domain Interaction within the Ryanodine Receptor in Ca^{2+} Channel Regulation. Trends Cardiovasc Med 2000;10:310–316. [PubMed: 11343972]
28. Shtifman A, Ward CW, Yamamoto T, et al. Interdomain Interactions within Ryanodine Receptors Regulate Ca^{2+} Spark Frequency in Skeletal Muscle. J Gen Physiol 2001;119:15–32. [PubMed: 11773235]
29. Oda T, Yano M, Yamamoto T, et al. Defective regulation of interdomain interactions within the ryanodine receptor plays a key role in the pathogenesis of heart failure. Circulation 2005;111:3400–10. [PubMed: 15967847]
30. Murayama T, Oba T, Kobayashi S, Ikemoto N, Ogawa Y. Postulated role of interdomain interactions within the type 1 ryanodine receptor in the low gain of Ca^{2+}-induced Ca^{2+} release activity of mammalian skeletal muscle sarcoplasmic reticulum. Am J Physiol Cell Physiol 2005;288:C1222–1230. [PubMed: 15677376]
31. Chu A, Diaz-Munoz M, Hawkes MJ, Brush K, Hamilton SL. Ryanodine as a probe for the functional state of the skeletal muscle sarcoplasmic reticulum calcium release channel. Mol Pharmacol 1990;37:735–41. [PubMed: 1692609]
32. Dulhunty AF, Laver DR, Gallant EM, Casarotto MG, Pace SM, Curtis S. Activation and Inhibition of Skeletal RyR Channels by a Part of the Skeletal DHPR II-III Loop: Effects of DHPR Ser687 and FKBP12. Biophys J 1999;77:189–203. [PubMed: 10388749]
33. Casarotto MG, Green D, Pace SM, Curtis SM, Dulhunty AF. Structural Determinants for Activation or Inhibition of Ryanodine Receptors by Basic Residues in the Dihydropyridine Receptor II-III Loop. Biophys J 2001;80:2715–2726. [PubMed: 11371447]
34. Green D, Pace S, Curtis SM, et al. The three-dimensional structural surface of two beta-sheet scorpion toxins mimics that of an alpha-helical dihydropyridine receptor segment. Biochem J 2003;370:517–27. [PubMed: 12429019]
35. Yamamoto T, El-Hayek R, Ikemoto N. Postulated Role of Interdomain Interaction within the Ryanodine Receptor in Ca^{2+} Channel Regulation. J Biol Chem 2000;275:11618–11625. [PubMed: 10766778]
36. Bannister ML, Hamada T, Murayama T, et al. Malignant hyperthermia mutation sites in the Leu2442-Pro2477 (DP4) region of RyR1 (ryanodine receptor 1) are clustered in a structurally and functionally definable area. Biochem J 2007;401:333–9. [PubMed: 16958617]
37. Tarroni P, Rossi D, Conti A, Sorrentino V. Expression of the ryanodine receptor type 3 calcium release channel during development and differentiation of mammalian skeletal muscle cells. J Biol Chem 1997;272:19808–13. [PubMed: 9242641]
38. Griggs RC, Jozefowicz R, Kingston W, Nair KS, Herr BE, Halliday D. Mechanism of muscle wasting in myotonic dystrophy. Ann Neurol 1990;27:505–12. [PubMed: 2360792]
39. Damiani E, Angelini C, Pelosi M, Sacchetto R, Bortoloso E, Margreth A. Skeletal muscle sarcoplasmic reticulum phenotype in myotonic dystrophy. Neuromuscul Disord 1996;6:33–47. [PubMed: 8845717]
40. Krivickas LS, Ansved T, Suh D, Frontera WR. Contractile properties of single muscle fibers in myotonic dystrophy. Muscle Nerve 2000;23:529–37. [PubMed: 10716763]

41. Barnes PR, Kemp GJ, Taylor DJ, Radda GK. Skeletal muscle metabolism in myotonic dystrophy A 31P magnetic resonance spectroscopy study. Brain 1997;120:1699–711. [PubMed: 9365364]

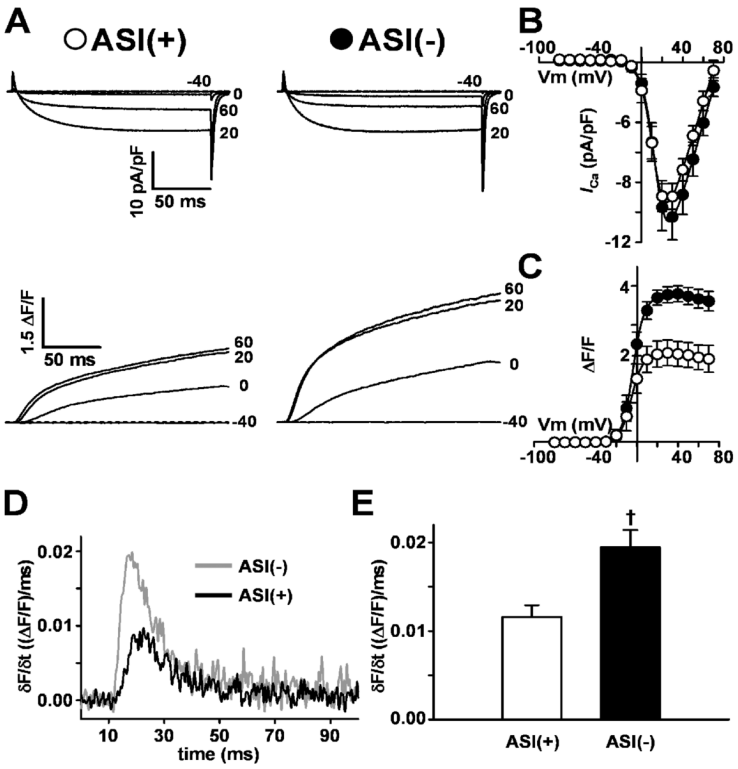

Figure 1. Maximal voltage-gated Ca^{2+} calcium release is enhanced in ASI(-)-expressing myotubes

A) Representative L-type Ca^{2+} currents (*upper traces*) and Ca^{2+} transients (*lower traces*) elicited by 200ms depolarisations to the indicated potential in ASI(+)RyR1- and ASI(-)RyR1-expressing myotubes. Average voltage-dependence of peak L-type Ca^{2+} current density (**B**) and intracellular Ca^{2+} transients (**C**) in dyspedic myotubes expressing ASI(+) (○, *n*=10) or ASI (-) (●, *n*=9). **D**) Representative time-dependence of the first derivative of the Ca^{2+} transient (δF/δt) elicited at +60mV in dyspedic myotubes expressing either ASI(+)RyR1 (*black trace*) or ASI(-)RyR1 (*grey trace*). **E**) Average peak of the first derivative of the Ca^{2+} transient (δF/δt) at +60mV in dyspedic myotubes expressing ASI(+)RyR1 (*open bar*) or ASI(-)RyR1 (*filled bar*). $^{\dagger}p<0.01$ compared to ASI(+)RyR1.

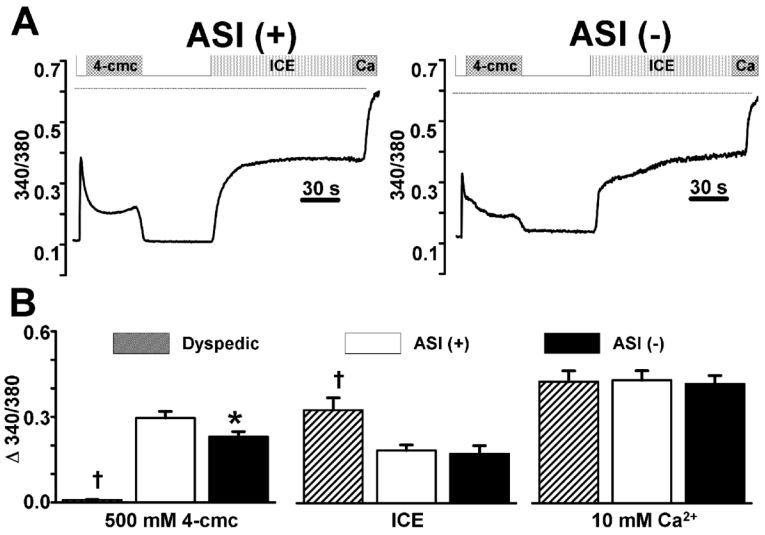

Figure 2. Releasable SR Ca^{2+} content is not different in ASI(+)RyR1- and ASI(-)RyR1-expressing myotubes

A) Representative fura-FF ratio (340/380) traces in ASI(+)RyR1- and ASI(-)RyR1-expressing myotubes following sequential addition of 500μM 4-cmc, wash, ICE (10μM ionomycin, 30μM CPA, and 2mM EGTA), and finally a 10mM Ca^{2+} + 10μM ionomycin Ringer's solution used to determine the maximal fura-FF ratio (*dotted lines*) during Ca^{2+} saturation of the dye. **B**) Average peak intracellular Ca^{2+} responses to addition of 4-cmc (*left*), 0 Ca^{2+} total store Ca^{2+} release cocktail (ICE, *middle*), and 10mM Ca^{2+} + 10μM ionomycin (*right*) in non-expressing (*hatched bars*, n=9), ASI(+)RyR1-expressing (*open bars*, n=29) and ASI(-)RyR1-expressing (*filled bars* n=22) dyspedic myotubes. $^{*}p<0.05$ compared to ASI(+)RyR1; $^{\dagger}p<0.01$ compared to ASI(+)RyR1. Minor deviations between the traces shown in **A** not observed in the average data reflect the cell-to-cell variability typically observed in these experiments.

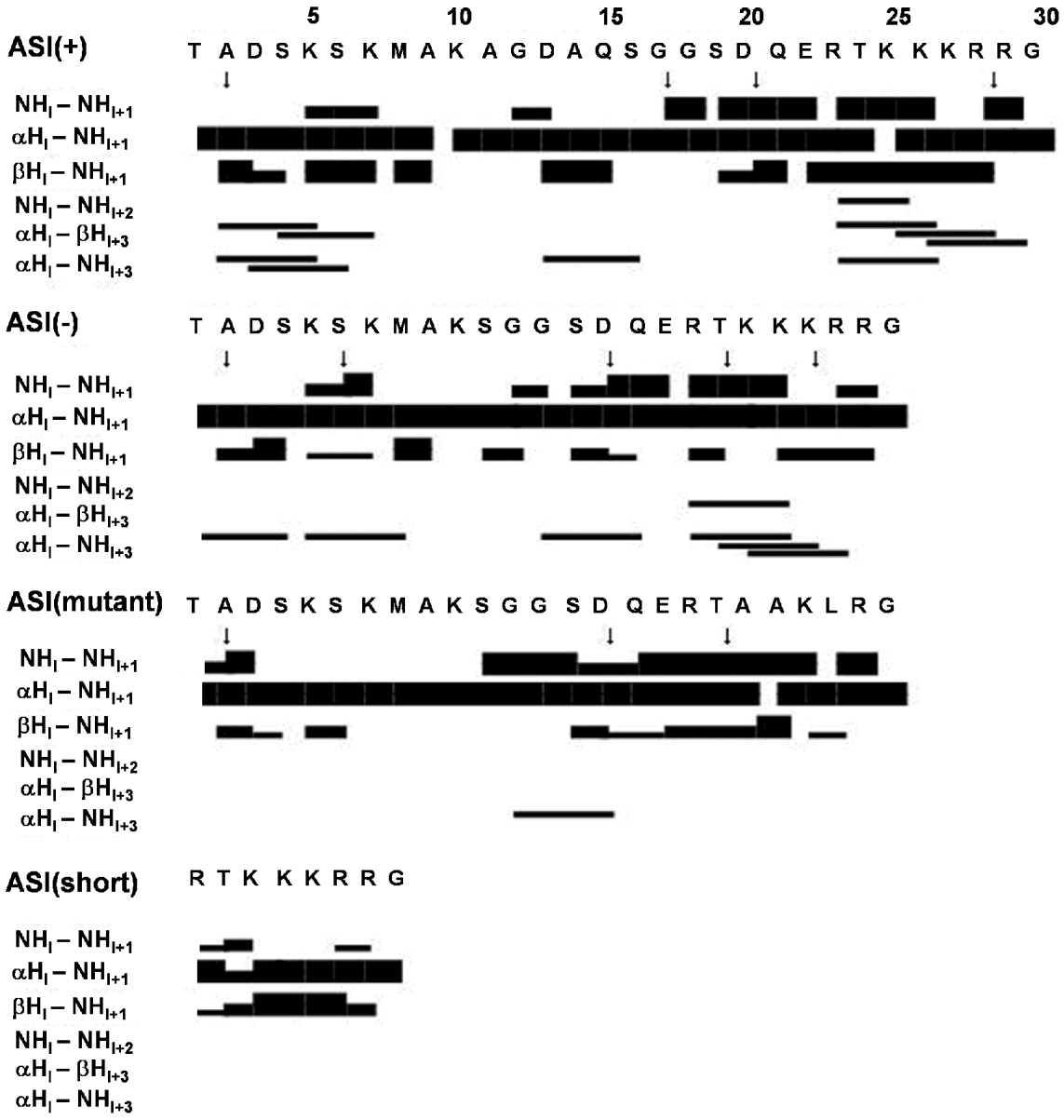

Figure 3. NMR-derived properties of the ASI peptides

Summary of the sequential and medium range connectivities, and $^{3}J_{NH\text{-}H\alpha}$ coupling constants identified for each of the ASI peptides. The NOE connectivities are indicated by black lines. The line thickness reflects the strengths of the NOE correlation as strong, medium and weak. Values of $^{3}J_{NH\text{-}H\alpha}$ less than 6 Hz are indicated by ↓.

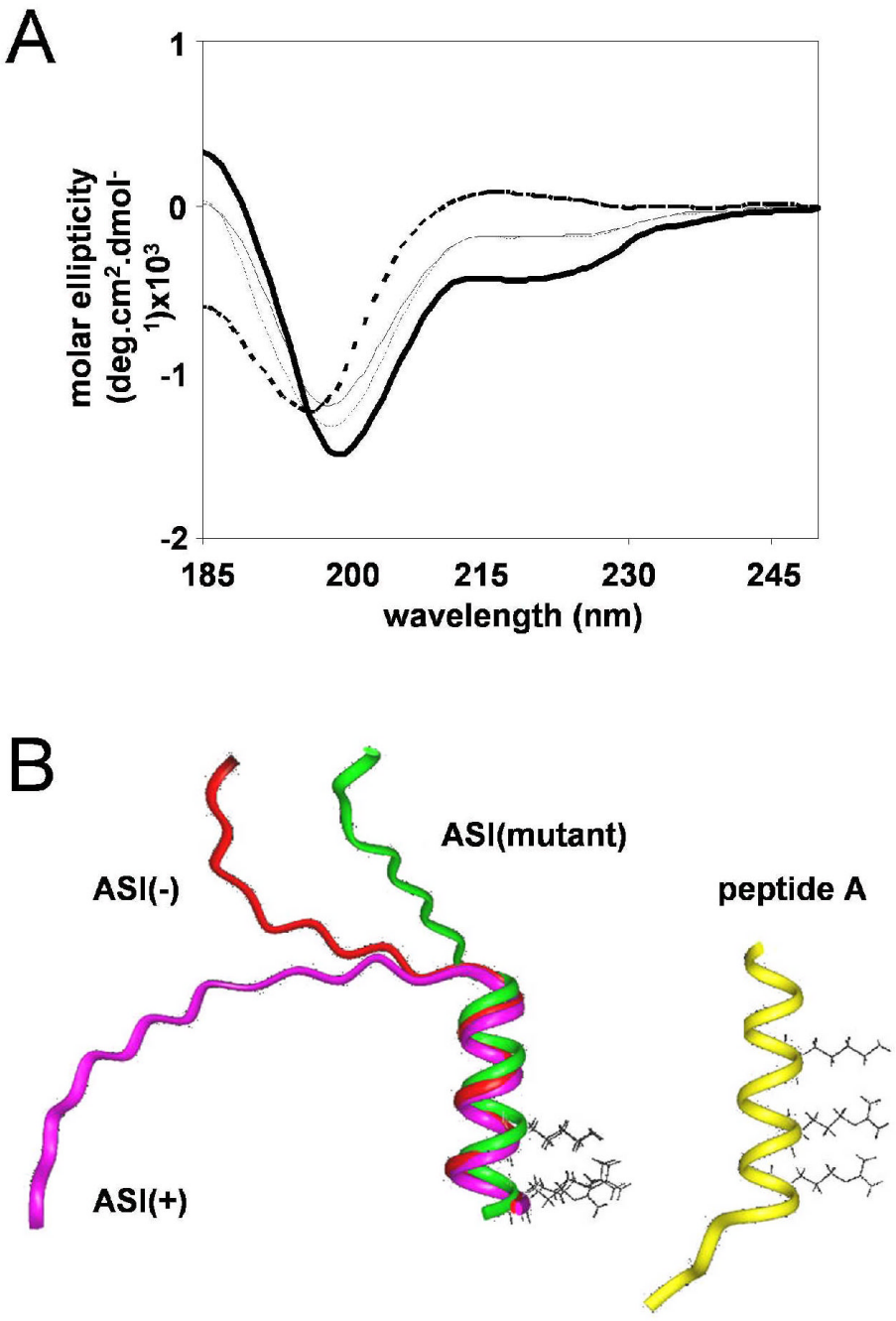

Figure 4. Structure of ASI peptides

A) CD spectra at 5°C for peptides ASI(+) (thin solid line), ASI(-) (thin dashed line), ASI(-) mutant (thick solid line), and ASI-short (thick dashed line) in H_2O, pH5.0. **B**) Structural representation of ASI(+), ASI(-), and ASI(-)-mutant (overlayed on left) and peptide ***A*** (right). Side chains of ASI residues K^{3495} and R^{3499} and peptide ***A*** residues K^{677}, R^{681} and R^{684} are indicated.

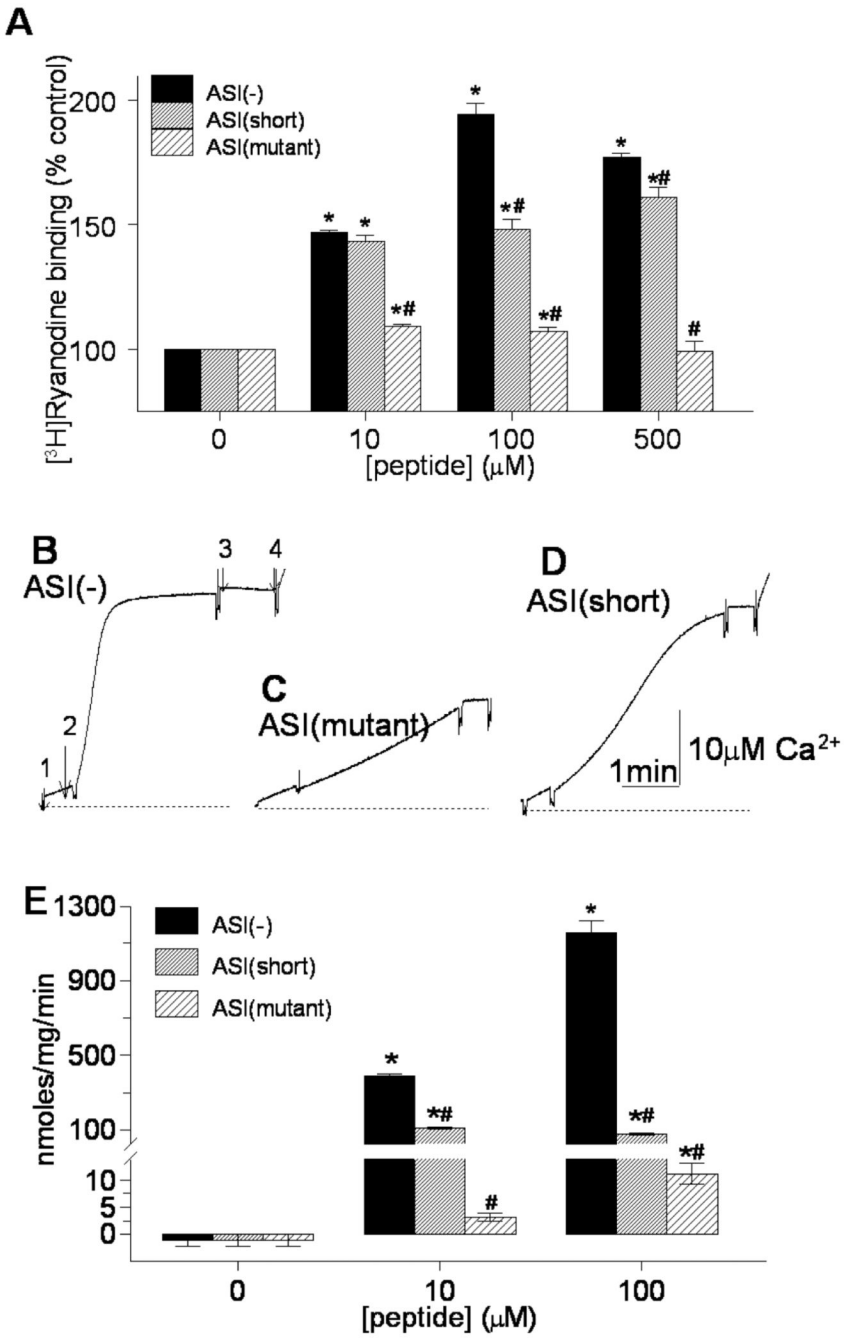

Figure 5. The sequence and structure of basic residues $K^{3495}KKRR^{3499}$ determines ASI peptide activation of RyR1

A) Effects of peptides ASI(-), ASI(mutant), and ASI(short) on [^{3}H]ryanodine binding with 10μM Ca^{2+} (n=3 for each peptide at each concentration). **B-D)** OD changes at 710nm, reflecting changes in extravesicular [Ca^{2+}] measured using antipyrylazoIII (500μM) with an addition of 1μM thapsigargin (first arrow), then 100μM peptide ASI(-)(second arrow in **B**), ASI(mutant) (**C**) or ASI(short) (**D**), 5μM ruthenium red (third arrow in **B**), and 1.5μg/ml Ca^{2+} ionophore A23187 (last arrow in **B**). **E**) Average rates (nmoles/mg/min, n=3) with peptides ASI(-), ASI(mutant), and ASI(short). The average initial rate of release (peptide minus thapsigargin) is shown in **E.** It is apparent in **D** that this initial rate is not substantially increased

by the ASI(short) peptide, while the later release rate (1-3min after peptide addition) is greater than that with ASI(mutant). Asterisks (*) in (**A**) and (**D**) indicate average values significantly different from control, while the ($^{\#}$) symbol indicates a significant difference from the wild-type ASI(-) at each peptide concentration.

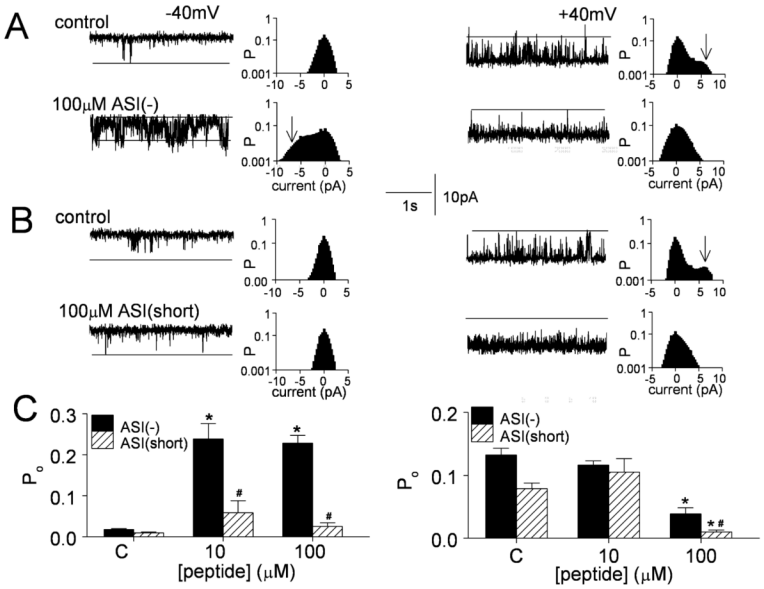

Figure 6. Peptide ASI(-) activates RyR1 channels at -40mV, but ASI(short) does not. Both peptides at 100μM inhibit channels at +40mV

A) & **B**) Channel activity (3s) with all-points histograms for the entire 30s record. The probability of the maximum open current (indicated by the broken lines in the channels records or arrows in the all-points histograms) is high only in the presence of ASI(-) at -40mV (in **A**) or under control conditions at +40mV in (**A** & **B**). Upper panels - control activity; lower panels - activity with 100μM peptide. **A**) ASI(-). **B**) ASI(short). Channel openings are downward at -40 mV (left) and upward at +40 mV (right). **C**) Average (n=3) effects of peptides ASI(-) and ASI-short on open probability of native RyR1 at -40mV (left) and +40mV (right). Asterisks (*) in (**C**) indicate average values significantly different from control (C), while the ($^{\#}$) symbol indicates values ASI(short) that are significantly different lower those with ASI(-) at the same peptide concentration.

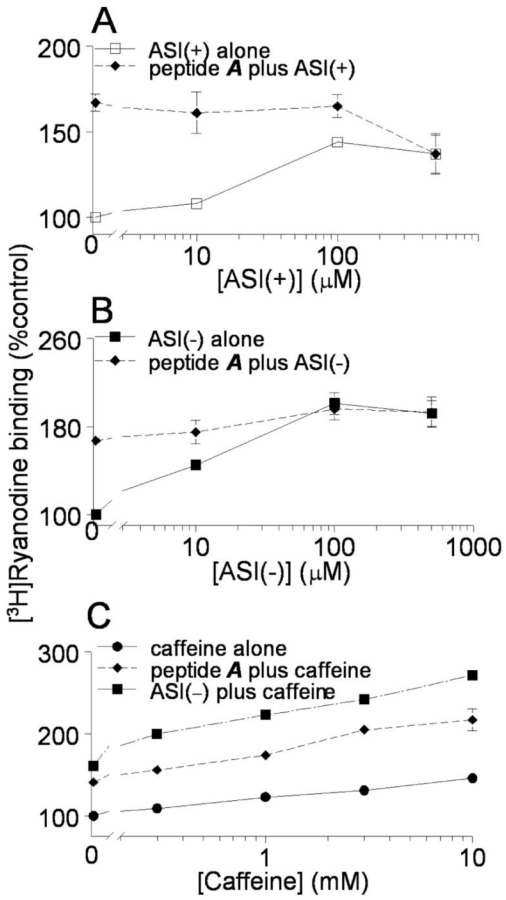

Figure 7. Competition between ASI peptides and peptide*A*

Relative [^{3}H]ryanodine with 10μM Ca^{2+}. **A)** ASI(+) alone (□) or ASI(+) plus 100μM peptide ***A*** (◆) with 10μM Ca^{2+}. Average values with ASI(+) alone are significantly greater than control at each peptide concentration. Peptide ***A*** produces a significant increase in activity, but there is not further increase as ASI(+)is added with peptide ***A***. **B**) ASI(-) alone (▪) or ASI(-) plus 100μM peptide ***A*** (◆) with 10μM Ca^{2+}. Average values with ASI(-) alone are significantly greater that control at each peptide concentration. Peptide ***A*** produces a significant increase in activity, but there is not further increase as ASI(-) is added with peptide ***A***. **C**) Caffeine alone (●) significantly increases [^{3}H]ryanodine at all concentrations tested. There is a further significant increase in activity each caffeine concentration when 100μM peptide ***A*** is present with caffeine (◆) and an additional significant increase when 100μM ASI(-) is present with caffeine (▪). Symbols show mean ±SEM (n=3). Some SEM bars do not appear because they fall within the dimensions of the symbols.

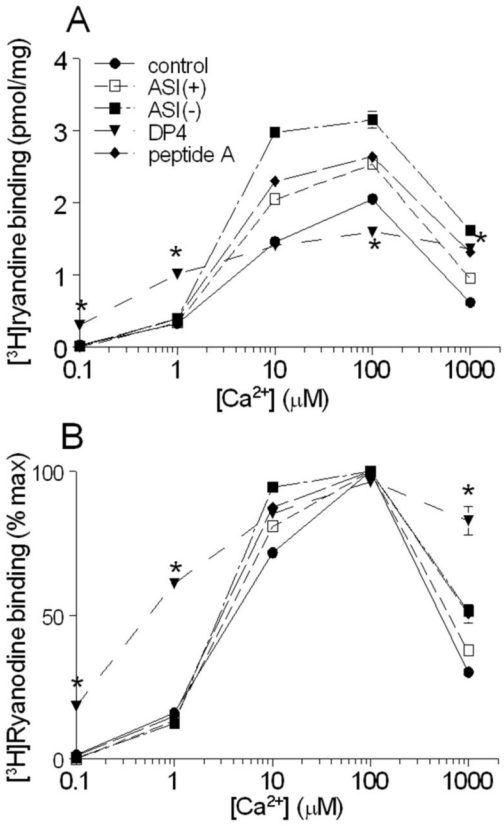

Figure 8. ASI peptides and peptide *A* do not alter the Ca^{2+}-dependence of [^{3}H]ryanodine binding

A) & **B**) Average (n=3) [^{3}H]ryanodine binding (**A**, pmol/mg; **B**, % maximum) in the absence of added peptide (●) or with 100μM ASI(+) (□),100μM ASI(-) (▪),100μM peptide ***A*** (◆), or 100μM DP4 (▼). In **A**), the average [^{3}H]ryanodine binding with each of ASI(-), ASI(+) and peptide ***A*** are significantly greater than that in the absence of peptide at Ca^{2+} concentrations ≥10μM. Amongst the 3 peptides, average [^{3}H]ryanodine binding with ASI(-) is significantly greater than with either ASI(+) or peptide ***A*** when Ca^{2+} was ≥10μM. Average [^{3}H]ryanodine binding with DP4 on the other hand is significantly greater than control with 0.1μM, 1.0μM and 1mM Ca^{2+}, no different with 10μM and significantly lower with 100μM Ca^{2+}. In **B**), there are no significant differences between the average normalised [^{3}H]ryanodine binding for control, ASI(-), ASI(+) and peptide ***A*** at any Ca^{2+} concentration. [^{3}H]ryanodine binding in the presence of DP4 is significantly higher than that with each of the other peptides in the presence of 0.1 μM, 1.0μM and 1mM Ca^{2+}. Some SEM bars do not appear because they fall within the dimensions of the symbols. Asterisks (*) indicate average [^{3}H]ryanodine binding with DP4 that is significantly different from values in the absence of peptide at the indicated Ca^{2+}.

Table 1

Parameters of Fitted I-V and F-V Curves

		I-V Data					F-V Data		
	N	**G_{max} (nS/nF)**	**k_G (mV)**	**$V_{G1/2}$ (mV)**	**V_{rev} (mV)**		**$(\Delta F/F)_{max}$**	**k_F (mV)**	**$V_{F1/2}$ (mV)**
ASI(-)	11	228±28	5.0±0.4	14.3±2.0	75.7±2.2		3.5±0.2†	4.3±0.3	-3.3±2.0
ASI(+)	13	214±14	5.1±0.2	14.4±1.8	72.7±2.2		2.2±0.7	3.5±0.3	-4.1±1.4

Mean ±SEM for *n* experiments. Parameters for the voltage dependence of Ca^{2+} current (*I-V*) and Ca^{2+} release (*F-V*) were obtained by fitting data from myotubes within each group separately to the appropriate equation [16]. G_{max}, maximal L-channel conductance; $(\Delta F/F)_{max}$, maximal change in relative fluo-4 fluorescence; V_{rev}, L-channel reversal potential; $V_{G1/2}$ and $V_{f1/2}$, potential at which G and F are half-maximal, respectively; k_G and k_F, slope factors for *I-V* and *F-V* curves, respectively.

† $p<0.01$ compared to ASI(+).